Analysis and modeling of a sea fog event over the Yellow Sea on 27 March 2005

Angeline Pendergrass
Department of Meteorology
University of Miami, Coral Gables, FL 33146

Mentor: Professor Gang Fu
Department of Meteorology
Ocean University of China, Qingdao, China 266003

Abstract

In this study, a sea fog event that occurred on 27 March 2005 over the Yellow Sea is investigated. Satellite imagery, station observations, NCEP reanalysis data and Regional Atmospheric Modeling System (RAMS) numerical simulation were used. Synoptic conditions and fog characteristics are described and analyzed to determine the physics behind the event. The fog formed when warm, moist air was advected northward over the cool water of the Yellow Sea. The fog dissipated when a cold front brought northerly winds and cool, dry continental air.

Visibility was determined by a post-processing calculation based on the mixing ratio of cloud liquid. The RAMS simulation did a reasonably good job of approximating the event.

Introduction

Fog occurs in many parts of the world. It is hazardous; it is blamed for accidents on sea and on land. Because it is a hazard, accurate forecasting is very important. But this requires a thorough understanding of the phenomena which has not yet been attained. Better understanding and forecasting ability of fog could improve maritime safety.

According to the American Meteorological Society (AMS), fog is "water droplets suspended in the atmosphere in the vicinity the earth's surface that affect visibility." It is basically a cloud whose base is at or near ground level (Aguado and Burt 2001). The maximum visibility for suspended water droplets to be considered fog is 1 km. The AMS says sea fog is "a type of advection fog formed when air that has been lying over a warm water surface is transported over a colder water surface, resulting in cooling of the lower layer of air below its dewpoint." The term is usually associated with moderate to dense fog (Koračin and Redmond 2004).

There have been reports on fog over or near the Yellow Sea. Fu et al. (2004) investigated the characteristics of fog over the Yellow and East China Seas. Cho et al (2000) documented historical data on sea fog and investigated the relation between sea fog occurrence and its environmental factors around the Korean Peninsula, which borders

the Yellow Sea to the east. There have also been investigations of fog using numerical modeling. Fan et al. (2003) did a fog simulation experiment with the National Center for Atmosphereic Research (NCAR)/Penn State mesoscale numerical prediction model (MM5) of advection fog in the Nanling mountain area. Pagowski et al (2004) investigated a dense fog event in southern Ontario using MM5.

This study investigated a sea fog event that occurred over the Yellow Sea on 27 March 2005. Satellite, land-based observations, and reanalysis data are used to determine the environmental conditions of the event. The event is simulated using the Regional Atmospheric Modeling System (RAMS). A detailed description of the most recent RAMS version is given by Cotton et al. (2003). The remainder of the paper is organized as follows. The second section details the sources of data and the methodology of the analysis. In the third section, an analysis of the environment during the event is presented. The fourth section deals with the numerical simulation. Finally, a brief discussion and conclusion is presented.

Data Sources and Methodology

Satellite

Geostationary Operational Environmental Satellite (GOES)-9 visible and infrared data were downloaded from Kochi University at weather.is.kochi-u.ac.jp. These data were used for the majority of the analysis during daytime hours. They are available every hourly during daylight. Darkness makes visible images useless and fog has no signature on infrared satellite, making its only use discerning the difference between clouds and fog on visible images. Visible satellite images do not show anything during the night, so satellite data is only useful during daylight hours. Daylight in the area of interest is from 00 UTC to 10 UTC. Local time is +8 UTC, so this corresponds to sunrise at 0800 LST and sunset at 1800 LST.

Observations

Station observations were obtained from the University of Wyoming (weather.uwyo.edu, older data can be requested). Data for 10 stations near the Yellow, Bohai, and East China Seas were used (figure 1). Station observations include visibility observation which is used to determine the presence of fog.

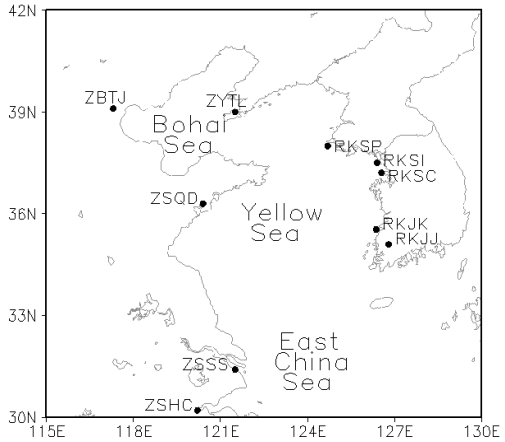

Figure 1. *Orientation map of analysis. Observing stations, area of focus, and bodies of water.*

Reanalysis

National Centers for Environmental Prediction (NCEP)'s Final run (FNL) analysis data were downloaded from University Corporation for Atmospheric Resaearch (UCAR) at dss.ucar.edu. The data are on a 1º horizontal grid with 26 vertical levels. Data are available every 6 h.

Variables examined in this study were geopotential height, zonal and meridional winds, temperature, relative humidity, surface pressure, sea level pressure, surface temperature, and 2-m temperature. These data were also used as initial conditions in the numerical simulation.

Upper air data

Radiosonde data from 5 upper air data stations taken at 6- or 12-h intervals (6 in South Korea and 12 in North Korea and China) was obtained from the University of Wyoming from 00 UTC 26 March to 12 UTC 28 March. Stations are listed in Table 2.

Table 1. Upper air data stations

Station number	**Identifier**	**Name**
54662	ZYTL	Dalian, China
54857	ZSQD	Qingdao, China
47122	RKSO	Osan Ab
47158	RKJJ	Kwangju Ab
47102		Baengnyeongdo

Computer programs

The Grid Analysis and Display System (GrADS) version 1.9 was used for data analysis and display and is available from the Institute of Global Environment and Society at http://grads.iges.org/grads/.

The Regional Atmospheric Modeling System (RAMS) was used to model the event. More details are available in section 4, which focuses on the numerical simulation.

Analysis and Results

The area analyzed in this project is the Yellow and Bohai Seas north of 35ºN and the adjacent land masses. This encompasses approximately 116ºE to 127ºE and 35ºN to 42ºN (shown in figure 1). The time period studied begins at 1200 Z 26 March, before the main patch of fog has developed, and ends 48 h later at 1200 Z 28 March, by which time the fog has cleared.

During the formation and most of the evolution of this event, clouds are present south of about 35ºN, making satellite data useless. When clouds are present, it is not possible to detect fog using satellite. Because of this, the analysis was restricted to the area north of 35ºN.

Observations

A look at satellite imagery gives us a general idea of how the event unfolded. At 00 UTC 26 March, low clouds are present over central Korea (though it is never detected at any of the observing stations) but the rest of the area of interest is free of clouds. At 03 UTC, a very small patch of what might be fog moves over the Yellow Sea and expands a little and moves northwest. When this patch reaches Dalian (ZYTL), it is detected as fog from 08 UTC to 10 UTC. Afterwards no fog is detected again until 17 UTC. This fog did not form over the sea originally so we did not consider it in our analysis.

The analysis begins just after nightfall (10 UTC) on 26 March at 12 UTC. At nightfall, the fog has not yet formed and is present at most as a small patch near Dalian. By the morning (00 UTC), fog covers almost the entire Yellow Sea and extends into low-lying areas on the adjacent land masses. Unfortunately, the formation of the fog is obscured by night in the satellite imagery. The fog is present all day on 27 March, and by morning on 28 March the fog in the northern part of the Yellow Sea has already dissipated. Satellite images from the duration of the event are shown in figure 2.

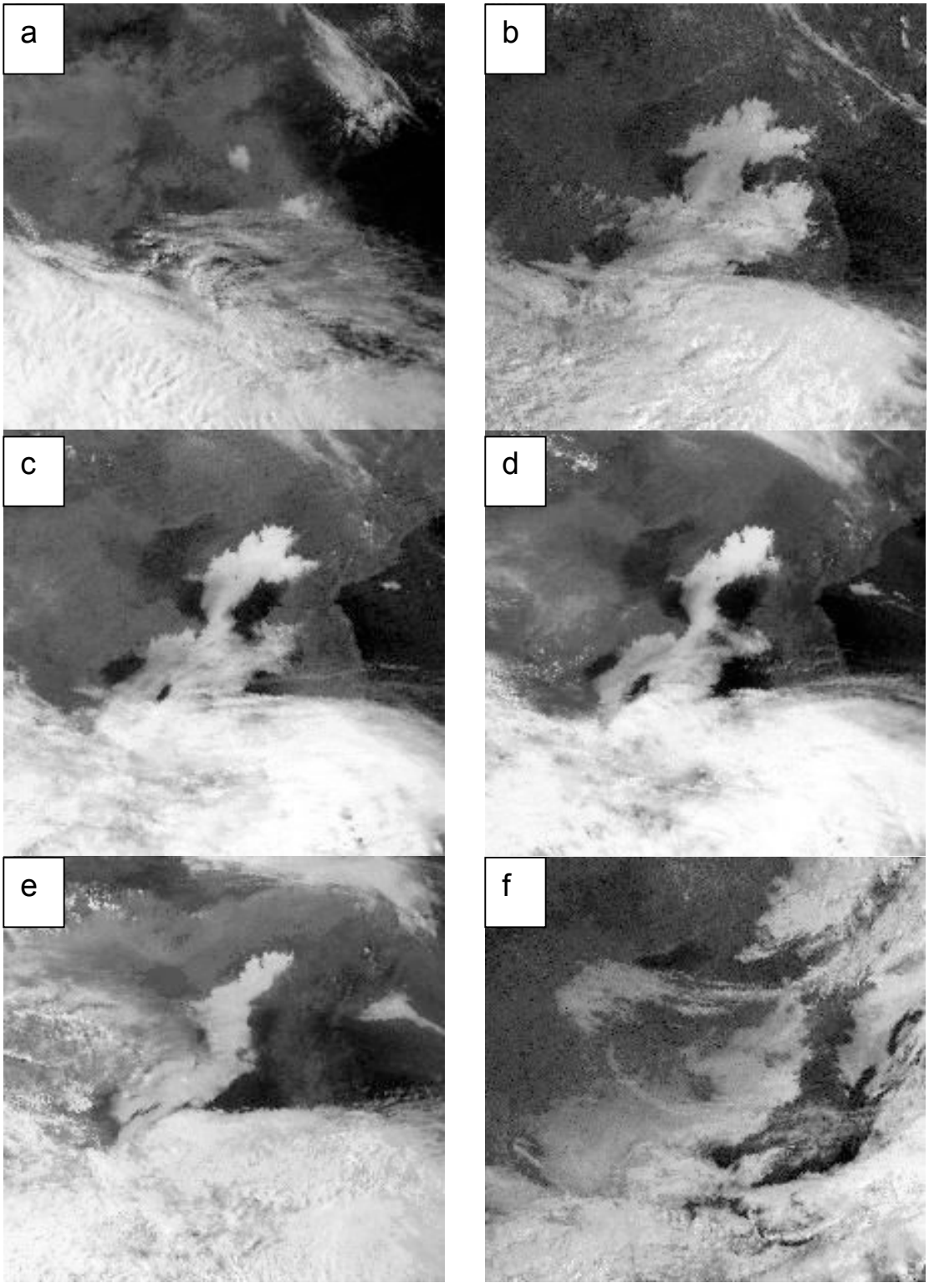

Figure 2. *Visible satellite imagery. a) 08 UTC 26 March b) 00 UTC 27 March c) 03 UTC 27 March d) 05 UTC 27 March e) 08 UTC 27 March f) 00 UTC 28 March*

In station observations, fog occurs when visibility is less than or equal to one kilometer. During the night when satellite imagery is not useful, the station observations are the only indication we have of the presence of fog. Fog is detected from 17 UTC 26 March until 01 UTC 27 March, at 11 UTC 27 March, from 1500 to 16 UTC 27 March, and 1900 to 22 UTC 27 March. It is only ever detected at 4 of to 10 stations for which data is obtained. Fog is not detected during most of the day on 27 March, which is when it is clear that fog is present over the sea from satellite data. However, visibility is low at Dalian all day on 27 March, just not low enough to be classified as fog. Visibility observed at Dalian (ZYTL) is shown in figure 3.

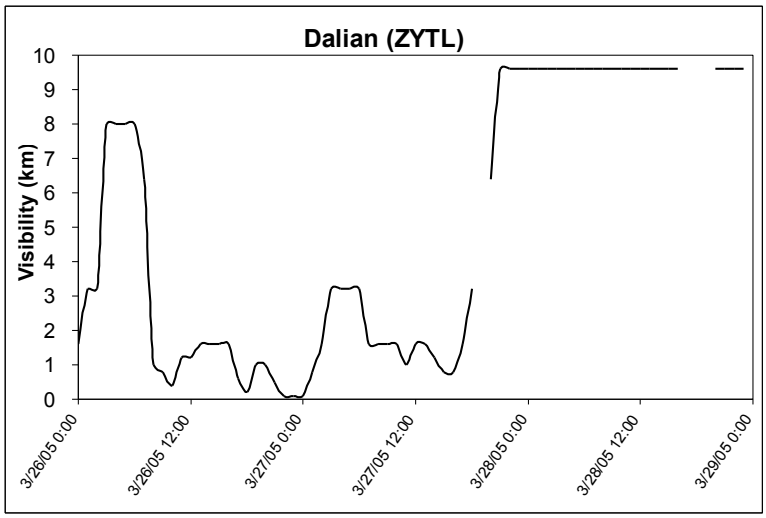

Figure 3. *Visibility (km) at observing station ZYTL for the duration of the event. Dalian reported fog more than any other station during the event.*

Stability

Atmospheric stability is an important environmental factor in the formation of fog. Fog forms only when the lowest part of the atmosphere is stable. Temperature and moisture data from radiosonde launches is examined to determine the stability of the atmosphere. Figure 4 shows sounding data from Qingdao and Dalian at 12 UTC 26 March.

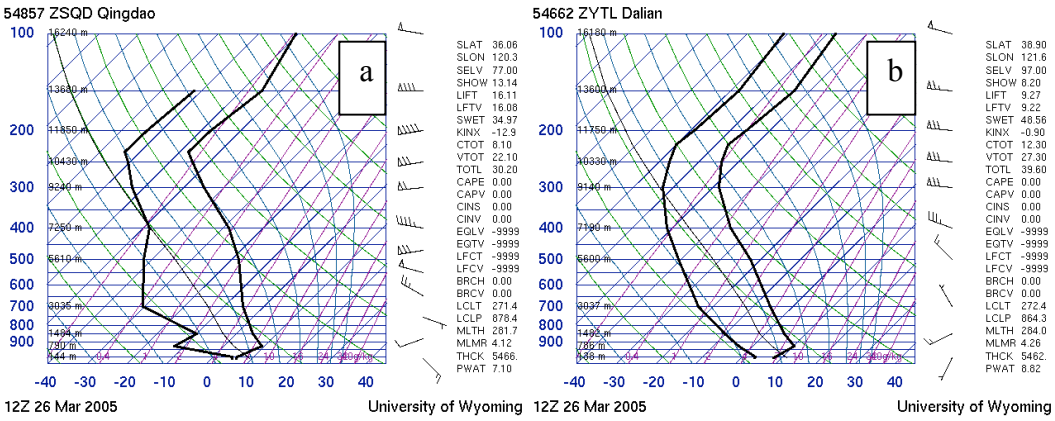

Figure 4. *Radiosonde data at 12 UTC 26 March at a) Qingdao and b) Dalian. The line on the left is the dewpoint temperature and the line on the right is the temperature (both in ºC). The wind barbs to the right of the skew-T log-P plot show the wind speed and direction every 50 hPa. The clockwise rotation with height in the lowest 150 hPa indicates warm air advection.*

Two important indicators of stability are the temperature profile and the convective available potential energy (CAPE). CAPE represents the energy available due to the buoyant force. The atmosphere is most stable when CAPE is zero. For all stations during the period of data, CAPE is zero, indicating that the atmosphere is convectively stable. The other indicator of a stable atmosphere is a temperature inversion, or an increase in temperature with height. A temperature in the lowest part of the atmosphere is a favorable environmental condition for fog formation. A temperature inversion is present below 900 hPa from 12 UTC 26 March until 12 UTC 28 March in Qingdao and Baengnyeongdo, and until 00 UTC 28 March in Dalian.

Formation

The first fog during our period of interest is detected in Dalian at 17 UTC 26 March. It is clear that the fog forms between 10 UTC (sunset) and 17 UTC on 26 March. Analysis of environmental conditions from the FNL reanalysis data will reveal the reasons for the formation of the fog.

A high pressure system just south of the southern tip of Japan and southeast of the Yellow Sea creates a southerly flow over the area of interest (not shown). The East China Sea, which is south of the Yellow Sea is the warmest of the bodies of water because it is fed by the warm Kuroshio Current. The Yellow Sea is much cooler, and the Bohai Sea is the coolest. So the southerly flow brings air that has been sitting over the warm East China Sea over the cooler water of the Yellow Sea (figure 5a). The southern air is also quite moist (not shown), so when the air is advected over the Yellow Sea, it is 0.5 to 3.5ºC warmer than the sea surface (figure 5b), and it cools to the dewpoint and fog forms. Sea fog usually occurs when the air temperature is 0.5 to 3.0ºC warmer than SST according to Fu et al. (2004).

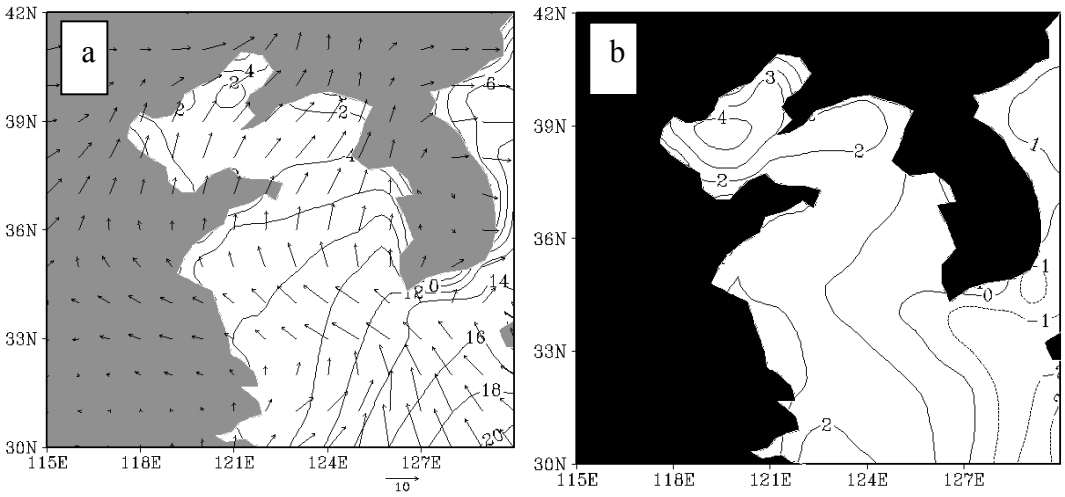

Figure 5. *Environmental conditions at 18 UTC 26 March. a) Winds superimposed over sea surface temperature (ºC) d) Surface temperature subtracted from 2-m temperature.*

Development

The fog is present throughout daylight hours on 27 March. According to the FNL data, the winds over the Yellow Sea are southerly between 2 and 10 m/s from 00 UTC to 12 UTC on March 27. Winds over the Bohai Sea are less uniform than those over the Yellow Sea. One interesting feature is an anticyclonic circulation present over the East China Sea. Its center is at 32º N 125ºE at 00 UTC, 33.5º N 126.5ºE at 06 UTC, and 33.5º N 127.5ºE at 12 UTC. Winds at 34 and 35º N are easterly at 00 UTC and change to northeasterly by 12 UTC on 27 March.

Warm air advection is poor and almost not present from 00 UTC 27 March on.

Dissipation

The fog begins to dissipate after 10 UTC on 27 March. A look at the reanalysis data shows a wind shift northeast of the Bohai Sea at 12 UTC 27 March. Behind this boundary, winds are from the north, bringing cool, dry air and cold air advection. The cold front is located between 38 and 39ºN from 115 to 124ºE. This cold front moves south and weakens, but is still strong enough to dissipate the fog. By 18 UTC 27 March, it is south of Dalian, and by 00 UTC 28 March, cold air advection has begun over the entire Yellow Sea (figure 6), ending the sea fog event.

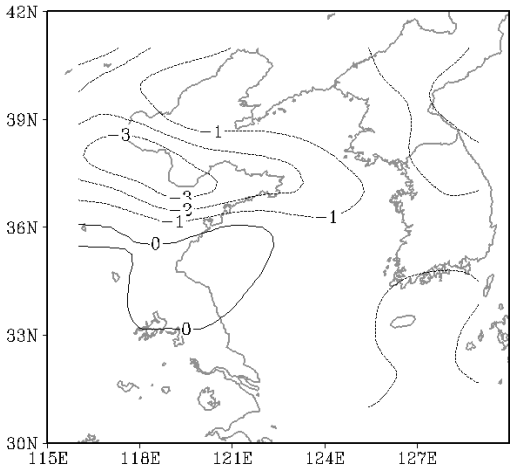

Figure 6. *Temperature advection (ºC s^{-1})*10000 at 00 UTC 28 March calculated from FNL data.*

Numerical Modeling

Specifications of RAMS 4.4 model run

To simulate the event, RAMS version 4.4 was used (Cotton et al. 2003). Table 1 shows the specifications of the model run. The simulation is useful for getting a detailed look at what might have happened during the sea fog event.

Table 2. Specifications of RAMS simulation

Category	**Specification**
Basic equation	Non-hydrostatic time-split compressible
Dimensionality	3-dimensional
Vertical coordinate	Terrain following height coordinate
Horizontal coordinate	Rotated polar-stereographic
Grid structure	240 x 240 x 30
Turbulence closure	Mellor-Yamada level 2.5 scheme (Mellor and Yamada, 1982)
Cloud microphysics	Level 3 -- Single-moment bulk scheme -- Walko et al (1995)
Convective	Modified Kuo-Tremback (1990)
Radiation	Chen and Cotton (1983) long/shortwave model
Lower boundary	Soil/vegetation parameterization -- LEAF-2 (Walko et al, 2000)
Lateral boundary	Klemp and Wilhelmson (1978) radiative condition
Initialization	FNL reanalysis data
Resolution	6 km x 6 km
Integration	48 h
Initial time	12 UTC 26 March 2005
Center	36ºN 120ºE
Surface Temperature	Updated every 6 h

Visibility calculation

Visibility is not predicted by the RAMS model, but it is used by observing stations to indicate fog. So, visibility is calculated from the mixing ratios of different

phases of water from RAMS as post-processing step. The calculation used comes from Stoelinga and Warner (1999). The extinction coefficient of a hydrometeor, β, depends on the mass concentrations, C, of the hydrometeor.

$$X_{vis} = -\ln (0.02)/\beta \quad (1)$$

$$\beta = \beta_{cw} + \beta_{ci} + \beta_{snow} + \beta_{rain} \quad (2)$$

Table 3. Calculation of visibility from mass concentration of hydrometeors.

Hydrometeor	**Relationship**	**Reference**
Cloud liquid water, fog	$\beta_{cw} = 144.7\ C^{0.88}$	(Kunkel, 1984)
Cloud ice	$\beta_{ci} = 163.9\ C^{0.88}$	(Rutledge & Hobbs, 1983)
Snow	$\beta_{snow} = 10.4\ C^{0.78}$	(Stallabrass, 1985)
Rain	$\beta_{rain} = 1.1\ C^{0.78}$	(Marshall-Palmer)

The only phase present during this event is cloud water.

Verification

Comparison of the visibility in the RAMS simulation with GOES visible satellite images was used to determine how closely the simulation approximates the event. The visibility field in the RAMS simulation closely follows the actual field over the Yellow Sea and on the coasts of Shandong province, Liaoning province, and Korea. The major difference between the simulation and the satellite data are that the simulation shows fog forming over the Bohai Sea while none was visible in satellite imagery. In the FNL data, the difference between the air temperature in the lowest layer and the sea surface temperature is greater in the Bohai Sea than in the Yellow Sea. In the model, they are about the same, though this may just be because fog has formed. In the Bohai Sea winds in the FNL data are from the southwest, or from the continent, while over the Yellow Sea they bring southern air directly from the warmer East China Sea. This difference in air mass plays a critical role. Aside from this, the simulation generally does a good job of showing fog at similar times and locations to those on the satellite. A comparison of these images is shown in figure 7.

The other place where the model simulation fails to follow the actual event is towards the end of the day on 27 March in the eastern part of the Yellow Sea. By 16 UTC 27 March, the eastern section of the patch of fog extending towards Korea has dissipated according the satellite imagery. In the simulation, it is still present and actually dissipates later than most of the rest of the fog.

The third downfall of the model is that according to the satellite data, the fog does reach onto the adjacent land in Liaoning province and the tip of Shandong province for all of 27 March, and into west central Korea during the morning. The model keeps the fog almost entirely over water.

The final downfall is that when the sun rises on 27 March (00 UTC), there is already one solid patch of fog, while two patches that formed separately have yet to merge in the model (figures 2b and 7a).

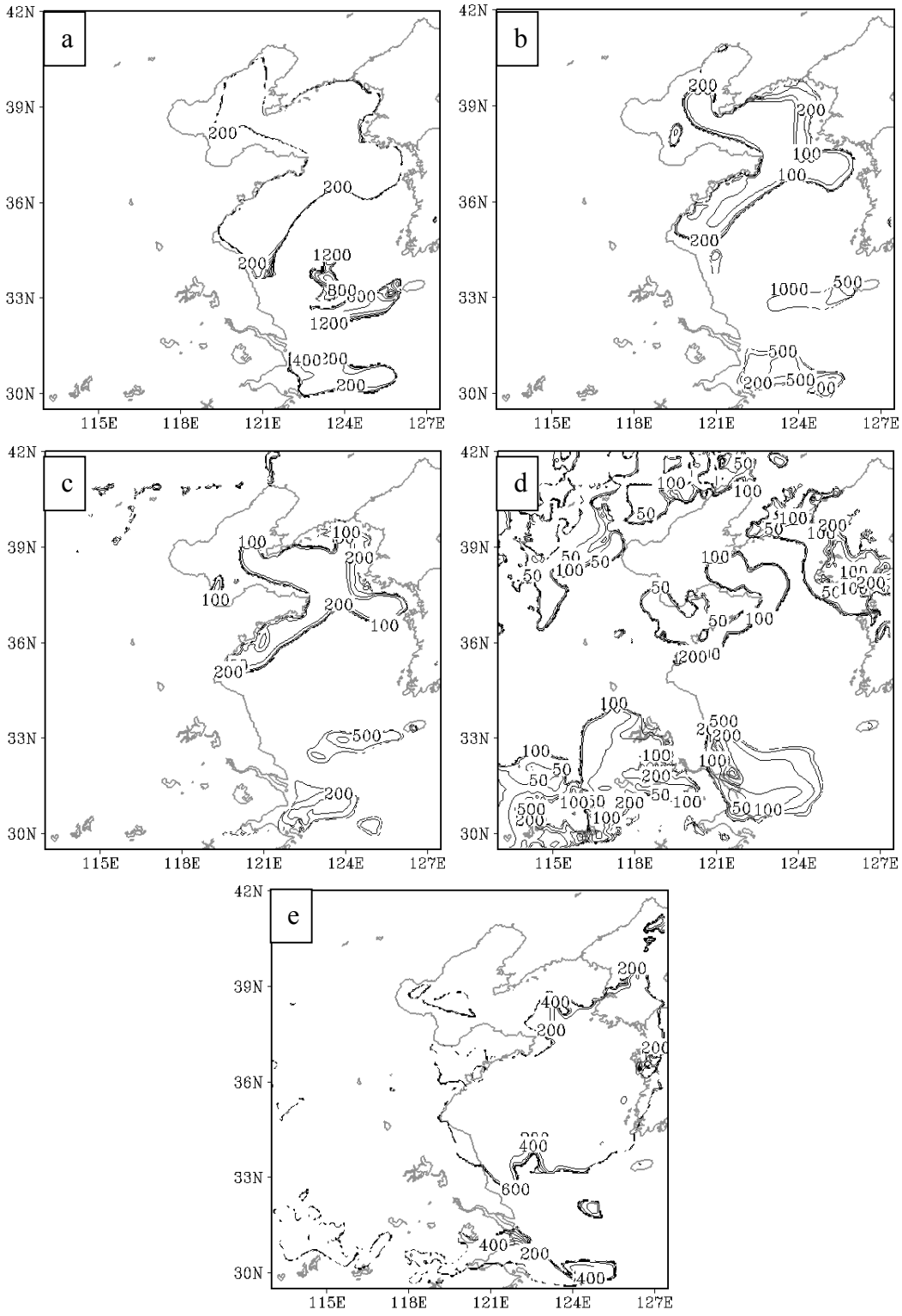

Figure 7. *Visibility (m) calculated from hydrometeor mass concentrations in the RAMS simulation. a) 00 UTC 27 March b) 03 UTC 27 March c) 05 UTC 27 March d) 08 UTC 27 March e) 00 UTC 28 March*

Overall, the model still does a reasonable job of simulating the fog event. It is useful to get an idea of how the event unfolded on a finer timescale than the reanalysis data and especially during the night, when satellite data is not useful.

The most useful model outputs are the mass concentrations of the various hydrometeors. Cloud liquid concentration is especially useful, because it can be considered as the actual concentration of fog (figure 8). The visibility obtained in post-processing is also very useful.

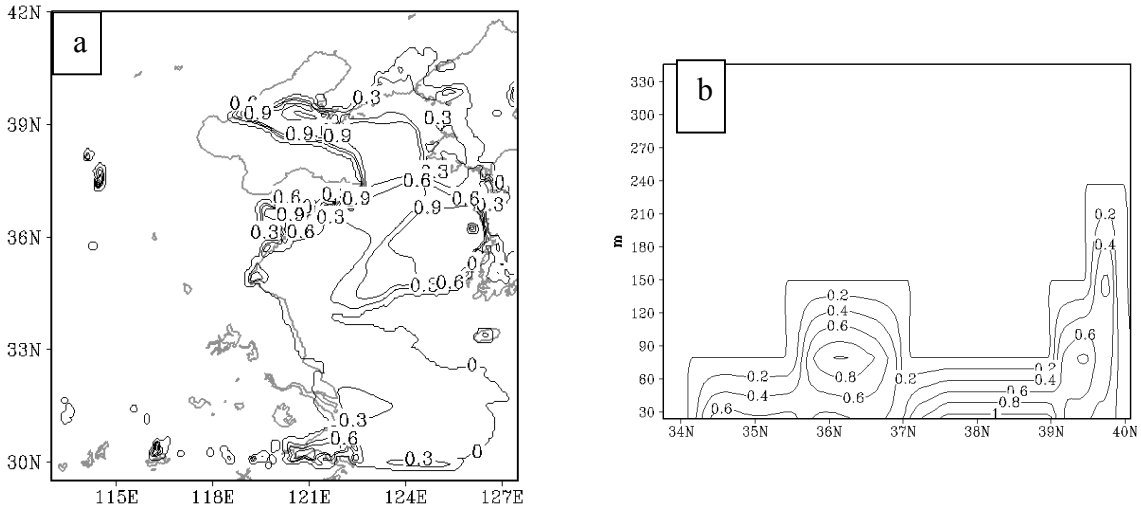

Figure 8. *Cloud mixing ratio from the RAMS simulation represents the actual fog at 18 UTC 27 March. a) Horizontal view b) Vertical cross section at 123ºE.*

Evolution of simulated event

The model begins at 12 UTC 26 March. Small pockets of fog form immediately over Liaoning province and western Korea. The first time patches of fog appear of water in the area of interest is at 17 UTC, just north of Shandong province. By 20 UTC, fog is developing north of Shandong and also south of the border between Korea and Liaoning. Both of these fog patches grow and by 02 UTC 27 March they merge together. At this point, the fog is also beginning to move over the Bohai Sea in the simulation. The fog continues to expand until 12 UTC, when it is covering the entire Yellow Sea and most of the northern part of the Bohai Sea with visibility of less than 50m, and some areas of fog with slightly more visibility extend over adjacent land.

By 19 UTC 27 March, the fog begins to recede. First, the fog south of the Shandong peninsula begins to fluctuate. Then the fog dissipates from north to south as a cold front moves south over the region (figure 6), despite that it weakens as it passes. At 00 UTC 28 March (when day breaks), fog is still present east and south of the Shandong peninsula, but it recedes promptly. By 04 UTC, the thickest fog is gone, and then only very small patches remain over the Yellow Sea.

A cross sectional analysis of cloud liquid water distribution at 123ºE, shown in figure 8b, is used to examine the vertical characteristics of the fog. The fog first forms

north of 39ºN at 19 UTC 26 March. By 22 UTC 26 March, the first fog patch has grown and a new fog patch forms between 37 and 38ºN. The southern patch remains less than 60 m in extent, vertically while the northern patch propagates upward (stopping below 200 m). As the densest part of the fog is sometimes are 80 m in some spots and as high as 150 m the northern patch, some of the fog may transition into low stratus. By 00 UTC 27 March, the northern patch is thickest at about 80 m while the southern patch remains below 60 m. The two patches merge at 03 UTC 27 March as they begin to thin from daytime heating. By 08 UTC 27 March, all of the fog is below 90 m and between 36 and 40ºN, and it has thickened again. By 12 UTC 27 March, the fog extend just south of 36ºN and north of 39ºN it extends to 120 m high. At 19 UTC 27 March it is at its largest extent, stretching from 34 to almost 40ºN. By 20 UTC 27 March, the northernmost fog begins to lift. By 22 UTC 27 March, all of the fog has thinned. By 01 UTC 28 March, only light fog is present anywhere, and by 02 UTC none is present at all.

Discussion and Summary

Data collected at land stations are sparse. A useful aid in the analysis of sea fog for future projects would be observations from ships.

The RAMS model did a very good job of modeling the fog, especially considering its coarse initial conditions. This might be because of the spatial scales of the factors in determining the fog's characteristics. The environmental conditions needed for fog, specifically a southerly wind field, ocean temperature decreasing to the north, and a stable atmosphere all occur for a longer time and over a larger interval than the reanalysis data. The factors that determine the spatial coverage of the fog are the ground surface and topography, which are built into the model on its 6-km grid spacing rather than the coarse reanalysis data.

On 27 March 2005, fog formed when warm, moist air was advected by southerly winds over the cooler water of the Yellow Sea. The fog persisted until a cold front passed early on 28 March, bringing cool, dry continental air. A simulation using RAMS did a reasonably good job of approximating the event, when the presence of fog is determined from visibility which is calculated from the cloud water variable in the model.

Acknowledgements

The author would like to acknowledge the program of the United States National Science Foundation Research Experience for Undergraduates in Marine Science and Engineering in China (NSF-China). This material is based upon work supported by the National Science Foundation under Grant No. OISE-0229657. Any opinions, findings, and conclusions or recommendations expressed in this material are those of the author(s) and do not necessarily reflect the views of the National Science Foundation.

Collaboration among scientists from around the world is important in today's increasingly global society. The opportunity to share cultural experiences and work side by side with scientists from other places is a valuable experience that the author

appreciates. This experience would not have been possible without the hard work of Hung Tao and Hayley Shen. The author would like to express thanks for the wonderful welcome to China of Professor Gang Fu and Miss Jingqian Wang.

References

Aguado, E., and J. Burt, 2001: *Understanding Weather and Climate*. Prentice Hall, total pages.

American Meteorological Society Glossary of Meteorology, Second Edition, Electronic Version (2000) http://amsglossary.allenpress.com/glossary

Chen, C., and W.R. Cotton, 1983: A one-dimensional simulation of the stratocumulus-capped mixed layer. *Bound.-Layer Meteor.*, **25**, 289–321

Cho, Y. K., M. O. Kim, and B. C. Kim, 2000: Sea Fog around the Korean Peninsula. *J. Appl. Meteor*., **39**, 2473-2479.

Cotton, W. R. and Coauthors, 2003: RAMS 2001: Current status and future directions. *Meteor. Atmos. Phys.,* **82**, 5-29

Crompton, J. G., 2003: Analysis and modeling of a sea fog event over the Yellow Sea on August 1, 2003. Report for REU in China.

Doty, B. and the Institute of Global Environment and Society, 2005: *The Grid Analsysis and Display System version 1.9.* COLA/IGES, Calverton, MD.

Fan, Q., A. Wang, S. Fan, D. Wu, X. Deng, and Y. Liu, 2003: Numerical prediction experiment of an advection fog in Nanling mountain area. *Acta Meteorologica Sinica*, **17**, 337-349.

Fu, G., M. Zhang, Y. Duan, T. Zhang, and J. Wang, 2004: Characteristics of Sea Fog over the Yellow Sea and the East China Sea.

GMS Data Archive for Research and Education. Kochi University. Available online at http://weather.is.kochi-u.ac.jp/archive-e.html

Holton, J.R., 1992: *An Introduction to Dynamic Meteorology*, Third Edition Academic Press, 511.

Klemp, J.B., and R.B. Wilhelmson, 1978: The Simulation of Three-Dimensional Convective Storm Dynamics. *J. Atmos. Sci.*, **35**, 1070–1096.

Lewis, J.M., D. Koračin, and K.T. Redmond, 2004: Sea Fog Research in the United Kingdom and United States: A Historical Essay Including Outlook. *Bull. Amer. Meteor. Soc.*, **85**, 395–408.

Kunkel, B.A., 1984: Parameterization of droplet terminal velocity and extinction coefficient in fog models. *J. Climate Appl. Meteor.*, **23**, 34-41.

Mellor, G.L., and T. Yamada, 1982: Development of a turbulence closure model for geophysical fluid problems. *Rev. Geophys. Space Phys.*, **20**, 851–875

NCEP Global Tropospheric Analysis (ds083.2). University Center for Atmospheric Research. Available online at dss.ucar.edu/datasets/ds083.2/

Oolman, L. (personal communication) Surface observations. University of Wyoming. Recent data online at http://weather.uwyo.edu/surface/meteogram/

Pagowski, M., I. Gultepe, and P. King, 2004: Analysis and modeling of an extremely dense fog event in southern Ontario. *J. Appl. Meteor.*, **43**, 3-16.

Rutledge, S.A., and P.V. Hobbs, 1983: The mesoscale and microscale structure and organization of clouds and precipitation in midlatitude cyclones. Part VIII: A model

for the "seeder-feeder" process in warm-frontal rainbands. *J. Atmos. Sci.*, **40**, 1185-1206.

Schoelinga, M.T., and T.T. Warner, 1999: Nonhydrostatic, Mesobeta-Scale Model Simulations of Cloud Ceiling and Visibility for an East Coast Winter Precipitation Event. *J. Appl. Meteor.*, **38**,385-404.

Stallabrass, J.R., 1985: Measurements of the concentration of falling snow. Preprints, Snow Property Measurements Workshop, Lake Louise, AB, Canada, National Research Council of Canada, 389-410.

Tremback, C.J.,1990: Numerical simulation of a mesoscale convective complex: Model development and numerical results. PhD Diss., Atmos Sci Paper No 465, Colorado State University, Department of Atmospheric Science, Fort Collins, CO 80523

Upper Air Data. University of Wyoming. Available online at http://weather.uwyo.edu/upperair/

Walko, R.L., C.J. Tremback, R.A. Pielke, and W.R. Cotton, 1995: An interactive nesting algorithm for stretched grids and variable nesting ratios. *J. Appl. Meteor.*, **34**, 994–999.

Walko, R.L., and Coauthors, 2000: Coupled atmosphere-biophysicshydrology models for environmental modeling. *J. Appl. Meteor.*, **39**, 931–944.